

# BROADBAND PHOTOMETRY OF 105 GIANT ARCS: REDSHIFT CONSTRAINTS AND IMPLICATIONS FOR GIANT ARC STATISTICS\*

MATTHEW B. BAYLISS

Department of Astronomy & Astrophysics  
Kavli Institute for Cosmological Physics  
The University of Chicago, Chicago, IL 60637

AND

Harvard-Smithsonian Center for Astrophysics  
Department of Physics and  
Harvard University, Cambridge, MA 02138

*Draft version February 1, 2018*

## ABSTRACT

We measure the photometric properties of 105 giant arcs that were identified in systematic searches for galaxy-cluster-scale strong lenses in the Second Red-Sequence Cluster Survey (RCS-2) and the Sloan Digital Sky Survey (SDSS). The cluster lenses span  $0.2 < z_l < 1.2$  in redshift, with a median  $\bar{z}_l = 0.58$ . Using broadband color criteria we sort the entire arc sample into redshift bins based on  $u-g$  and  $g-r$  colors, and also  $r-z$  colors for the  $\sim 90\%$  of arcs that have  $z$ -band data. This analysis yields broad redshift constraints with  $71^{+5}_{-4}\%$  of the arcs at  $z \geq 1.0$ ,  $64^{+6}_{-4}\%$  at  $z \geq 1.4$ ,  $56^{+5}_{-4}\%$  at  $z \geq 1.9$ , and  $21^{+4}_{-2}\%$  at  $z \geq 2.7$ . The remaining  $29^{+03}_{-5}\%$  have  $z < 1$ . The inferred median redshift is  $\bar{z}_s = 2.0 \pm 0.1$ , in good agreement with a previous determination from a smaller sample of brighter arcs ( $g \lesssim 22.5$ ). This agreement confirms that  $z_s = 2.0 \pm 0.1$  is the typical redshift for giant arcs with  $g \lesssim 24$  that are produced by cluster-scale strong lenses, and that there is no evidence for strong evolution in the redshift distribution of arcs over a wide range of  $g$ -band magnitudes ( $20 \leq g \leq 24$ ). Establishing that half of all giant arcs are at  $z \gtrsim 2$  contributes significantly toward relieving the tension between the number of arcs observed and the number expected in a  $\Lambda$ CDM cosmology, but there is considerable evidence to suggest that a discrepancy persists. Additionally, this work confirms that forthcoming large samples of giant arcs will supply the observational community with many magnified galaxies at  $z \gtrsim 2$ .

*Subject headings:* gravitational lensing — galaxies: high-redshift galaxies — cosmology: observations — large-scale structure of universe

## 1. INTRODUCTION

The statistics of strong gravitational lensing by clusters of galaxies provides a test of cosmological models, by comparing the observed abundance of giant arcs against predictions from ray-tracing cosmological N-body simulations. Incidents of strong lensing are often identifiable by the formation of giant arcs, which are background sources that are strongly lensed into multiple, often merging, images by a foreground gravitational potential. The frequency of giant arcs is a complex observable that scales with the halo mass

function, the detailed properties of high-redshift galaxy population, and the internal properties of the halos (e.g., Grossman & Narayan 1988; Bartelmann et al. 1998; Cooray 1999; Gilmore & Natarajan 2009). Bartelmann et al. (1998) first suggested that the number of giants arcs on the sky is under-predicted by  $\Lambda$ CDM by approximately an order of magnitude, and later observational comparisons using small samples of giant arcs corroborated the apparent over-abundance of giant arcs on the sky compared to  $\Lambda$ CDM predictions (Luppino et al. 1999; Zaritsky & Gonzalez 2003; Gladders et al. 2003; Li et al. 2006). In principle, it should be possible to produce predictions for giant arc statistics that match what we observe, assuming that we possess a suitably accurate model describing the formation and evolution of structure over cosmic time. In practice, the apparent failure of predictions for giant arc statistics to match the observations by as much as an order of magnitude is clear evidence that more work remains to be done.

Resolving the persistent discrepancy between the abundance of giant arcs observed and the number predicted by early simulation efforts requires progress on two fronts: 1) improved empirical constraints from much larger samples of giant arcs that are identified in uniform data with a well-characterized selection, and 2) refined

mbayliss@cfa.harvard.edu

\* Based on observations taken at the Southern Astrophysical Research Telescope (SOAR), a collaboration between CNP-Brazil, NOAO, The University of North Carolina at Chapel Hill, and Michigan State University and the Canada-France-Hawaii Telescope (CFHT) on Mauna Kea, which is operated by the National Research Council of Canada, the Institut National des Sciences de l'Univers of the Centre National de la Recherche Scientifique of France, and the University of Hawaii. Additional supporting observations come from the 2.5m Nordic Optical Telescope, operated on the island of La Palma jointly by Denmark, Finland, Iceland, Norway, and Sweden, in the Spanish Observatorio del Roque de los Muchachos of the Instituto de Astrofísica de Canarias, and the Gemini Observatory, which is operated by the Association of Universities for Research in Astronomy, Inc., under a cooperative agreement with the NSF on behalf of the Gemini partnership: The United States, The United Kingdom, Canada, Chile, Australia, Brazil and Argentina

predictions based on simulated giant arc samples. It is tempting to consider the possibility of giant arc statistics providing direct observational evidence for divergence from the concordance  $\Lambda$ CDM cosmology (Fedeli et al. 2008; D’Aloisio & Natarajan 2011), but we must first explore other physical explanations for the discrepancy between giant arc counts in observations and simulations. Motivated by the Bartelmann et al. (1998) result, theoretical work over the past decade has explored a variety of effects which, if unaccounted for in theoretical predictions, can result in an under-abundance of simulated arcs compared to the number of giant arcs observed in the real universe.

Suggested effects include the contribution of baryons to cluster lensing cross-sections in the form of central massive galaxies and substructure (Flores et al. 2000; Meneghetti et al. 2000, 2003; Hennawi et al. 2007; Meneghetti et al. 2010), the effects of dark matter being dragged into the cores of clusters by cooling baryons (Puchwein et al. 2005; Rozo et al. 2008; Wambsganss et al. 2008), triaxiality of cluster mass profiles (Oguri et al. 2003; Dalal et al. 2004; Hennawi et al. 2007; Meneghetti et al. 2010), accounting for additional but uncorrelated structure in the universe that is projected along the line-of-sight of lens-source systems (Wambsganss et al. 2005; Hilbert et al. 2007; Puchwein & Hilbert 2009), short time-scale increases in the strong lensing cross-section due to major mergers (Torri et al. 2004; Fedeli et al. 2006; Hennawi et al. 2007), and the properties of the assumed background galaxy source population (Hamana & Futamase 1997; Wambsganss et al. 2004). The aforementioned papers have generally quantified the impact of various effects in the context of comparing predictions and observations for the frequency of the formation of giant arcs, with several authors making arguments to disclaim the discrepancy noted by Bartelmann et al. (1998) (e.g., Wambsganss et al. 2004; Horesh et al. 2005, 2011). These arguments, however, are based on the identification of *possible* mechanisms for explaining or alleviating the apparent giant arc discrepancy, and there is a persistent lack of empirical evidence to confirm or deny the relevance of these different mechanisms.

### 1.1. *The Background Source Population*

In this paper we focus on the background galaxy population as an input into predictions for giant arc abundances in simulations, and make a direct measurements of the giant arc redshift distribution for a large sample of real giant arcs. Evidence from theoretical work (Wambsganss et al. 2004) suggests that the use of appropriate distribution of background galaxies may have the greatest potential to explain the dramatic discrepancy between the giant arc counts observed and those predicted by simulations in a  $\Lambda$ CDM cosmology. The redshift distribution of background sources impacts the global efficiency for giant arc production through the angular diameter distance term in the gravitational lens equation (Equ. 13, Narayan & Bartelmann 1996), which has an explicit dependence on the ratio of the angular diameter distances between the lens and the source, and the observer and the source. In practice, this means that the critical surface mass density for a given foreground lens is a function of the source redshift, where higher

source redshifts result in lower critical surface mass densities. When analyzing the total cross section for strong lensing of all clusters within some cosmological volume, a background source population that is shifted to higher redshifts will therefore require lower surface mass densities of foreground structures in order to become supercritical (i.e. to be strong lenses). There has, however, been little effort made to systematically measure the background source redshift distribution of a well-defined sample of arcs until very recently. Bayliss et al. (2011a) first measured the redshift distribution for a spectroscopically complete sample of 28 giant arcs that were observed with Gemini-South, and they demonstrate that the giant arc redshift distribution can only be reliably measured using a large sample of uniformly selected giant arcs.

Wambsganss et al. (2004) note an increase in the total strong lensing cross-section for galaxy cluster-scale lenses of a factor of  $\sim 10 - 20$  when the background sources that are lensed into giant arcs are assumed to be at corresponding source planes of  $z_s = 1.5 - 2$  rather than  $z_s = 1$ . Other work in which this effect is quantified finds smaller increases in the strong lensing cross-section by a factor of  $\sim 3$  or so (Dalal et al. 2004; Li et al. 2005; Fedeli et al. 2006), but this still implies a significant potential boost in the total cross-section for giant arc production if giant arcs are typically formed by lensing of galaxies at  $z_s = 2$ , rather than the  $z_s = 1$  source population used by Bartelmann et al. (1998). The importance of understanding the properties of the background source population that is lensed into arcs is further highlighted by more recent simulation work to generate predictions for giant arc statistics.

In agreement with early semi-analytic arguments (Oguri et al. 2003), Hennawi et al. (2007) identify the dominant uncertainty in their ability to robustly predict giant arc counts to be the poor constraints on the number density of galaxies at high redshift that are available to be strongly lensed by foreground cluster lenses. This uncertainty is fundamentally a reflection of our ignorance of the faint tail of the surface brightness function of galaxies at high redshifts. When we consider the implications of Wambsganss et al. (2004) and Hennawi et al. (2007) together it becomes clear that we cannot realistically make any useful statements about cosmology from tests of giant arc statistics without a firm understanding of the population of galaxies that are typically lensed into giant arcs.

The first spectroscopic measurement of the redshift distribution for a complete sample of well-selected giant arcs indicates a median arc redshift of  $\bar{z}_s = 1.82$  (Bayliss et al. 2011a). However, the sample used in that work was still relatively small ( $N_{arcs} = 28$ ), and potentially biased toward high-redshift giant arcs due to a target selection criteria which favored larger giant arc radii ( $R_{arc}$ ) systems, where  $R_{arc}$  is the average angular distance between an arc and the centroid of the foreground lensing potential. There should be a net correlation between  $R_{arc}$  and the intrinsic Einstein radius,  $R_E$ , of a given lens, and for a given lens the Einstein radius grows monotonically with the redshift of the lensed source. However, there should also be a large scatter in the correlation between  $R_{arc}$  and  $R_E$  that could easily be washed out by other factors such as the shape of the critical curves for each individual lens. It is not clear to what degree this potential

selection bias should impact the results of Bayliss et al. (2011a), but there is a somewhat reasonable argument to be made that the redshift distribution measurement in Bayliss et al. (2011a) could be biased significantly high. In order to ensure a robust understanding of the properties of the galaxies that are typically lensed into giant arcs, it is important that we extend these investigations further to incorporate very large sample of arcs that are not subject to the same selection effects as those in Bayliss et al. (2011a). However, measuring spectroscopic redshifts for a sample of  $\sim 100$  giant arcs is extremely observationally expensive, especially in a scenario where spectroscopic completeness (i.e. redshift measurements for  $\sim 100\%$  of the observed sample) is important.

We also note that counting giant arcs may be in large part free from the issue of magnification bias that is known to affect, for example, counts of unresolved galaxies or quasars behind foreground lensing structures (Broadhurst et al. 1995). As Dalal et al. (2004) point out, the magnification due to gravitational lensing is spatial in nature, with surface brightness a conserved quantity. The magnification does not, therefore, impact the number density of spatially resolved objects on the sky. Giant arcs are always, by definition, spatially resolved along at least one (and sometimes both) axis(es) on the sky. Assuming that magnification bias does not strongly influence counts of giant arcs, we make no attempt to model or correct for the affect in this paper. In support of this assumption we note that § 4.2 includes a direct comparison of the median redshifts of two samples of giant arcs that were selected from imaging data that different in depth by  $\sim 1.5 - 2$  magnitudes. The observed similarity in the median redshifts of these two samples provides some empirical evidence to support the argument that magnification bias does not strongly impact surveys of giant arcs, but future arc searches that probe to fainter magnitudes will be necessary to robustly quantify the precise effect of the magnification bias on giant arc counts.

### 1.2. Measuring the Properties of A New Giant Arc Sample

The “giant arc problem” posed by the apparent excess of giant arcs on the sky relative to  $\Lambda$ CDM predictions persists because of limitations on both the theoretical predictions and observational constraints. Making serious progress toward addressing the issue requires improving the fidelity of the machinery for theoretical predictions, which has been progressing steadily in recent years, but it also demands improvement on the observational side with respect to defining useful observational samples for comparison against the best predictions that theory has to offer. To that end, we have undertaken a systematic search for giant arcs around optically selected clusters in two large imaging surveys: the Second Red Sequence Cluster Survey (RCS-2; Gilbank et al. 2011) and the Sloan Digital Sky Survey (York et al. 2000). An exhaustive visual inspection of these two surveys has produced a combined sample of hundreds of uniformly selected giant arcs (M. D. Gladders et al. 2011, in preparation; M. B. Bayliss et al. 2011, in preparation). Complete definition of these samples (completeness, purity, effective area/volume probed) will be forthcoming in future work, but even prior to the completion of the sample

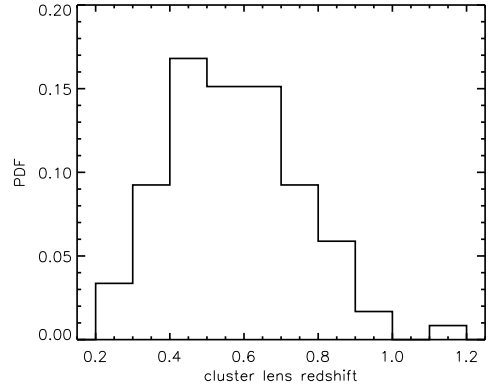


FIG. 1.— The probability distribution of photometric redshifts for the population of foreground galaxy clusters that are responsible for producing the giant arcs analyzed in this paper.

definition there is a tremendous amount to be learned by characterizing the properties of the giant arcs themselves.

In this paper we use photometric color criteria to sort a uniformly-selected sample of 105 arcs into four redshifts bins at  $z > 1$ , and evaluate the implications of the resulting arc redshift distribution. The redshifts and linear arc brightnesses of the sample are two observables that can be measured directly from the data, and used to inform future efforts to generate simulation-based predictions of giant arc abundances and match them to our new large giant arc samples. As discussed above, we can also provide direct insight regarding a possible resolution of the “giant arc problem” by definitively establishing that most giant arcs are galaxies that reside at high redshift (i.e.  $z \gtrsim 2$ ).

This paper is organized as follows: in § 2 we summarize the photometric and spectroscopic data analyzed in this paper. § 3 describes our analysis methods, including aperture photometry of giant arcs and the color-based sorting of giant arcs into broad redshift bins. In § 4 we summarize the state of the current literature regarding investigations into possible contributing factors to the “giant arc problem”, and discuss the implications of our results.

All magnitudes presented in this paper are calibrated relative to the AB system, via the SDSS.

## 2. OBSERVATIONS

### 2.1. Giant Arcs Targeted for $u$ -band Observations

The objects analyzed in this paper are drawn from a pair of comprehensive surveys for giant arcs in the RCS-2 and SDSS survey imaging data. As a part of a larger collaboration, we have systematically searched the RCS-2 and SDSS DR7 (Abazajian et al. 2009) for incidences of strong lensing by galaxy clusters. The search is performed by identifying lines-of-sight in the optical survey data which are likely to contain galaxy clusters using the red-sequence algorithm (Gladders & Yee 2000, 2005). The red-sequence cluster finding identifies over-densities of red galaxies on the sky, and provides photometric redshift estimates for the galaxy clusters from the redshifted  $4000\text{\AA}$  break. The galaxy cluster samples from the RCS-2 and SDSS DR7 span redshift ranges of  $0.2 \lesssim z \lesssim 1.2$  and  $0.2 \lesssim z \lesssim 0.65$ , respectively.

In order to identify strong lenses, each optically selected galaxy cluster is independently inspected by multiple experts and scored for evidence of strong lensing. Inspectors are also randomly made to re-score lines-of-sight that they have already scored, thereby providing data that will be used to quantify the consistency of our scoring, as well as our final completeness as a function of the averaged scores. We have also conducted exhaustive follow-up observations to quantify the purity of the resulting sample as a function of average score. A complete description of the SGAS and RCSGA samples are forthcoming (M. D. Gladders et al., in preparation, and M. B. Bayliss et al., in preparation, respectively). The giant arcs used in this paper are located around 97 unique galaxy clusters that span the full range in photometric redshifts of the parent catalog of optically selected clusters described just above, with a median lens redshift of  $\bar{z}_l = 0.58$ . In Figure 1 we show the the probability distribution of foreground cluster lens redshifts for the giant arc sample.

The giant arc sample presented in this paper is an *incomplete* subset of the full SDSS and RCS-2 giant arc samples. In the paper we analyze photometric data for 105 systems which constitute a large fraction of the final combined SGAS + RCSGA samples. The criteria for inclusion in our analysis here are: 1) the giant arc was identified in a systematic search of  $g$ -band imaging with depth matching the limits of the RCS-2  $g$ -band survey data, and 2) that we possess photometric  $u$ -band imaging of that arc. The  $u$ -band data is essential for classifying giant arcs based on well-established photometric dropout criteria for distant blue galaxies (e.g., Steidel et al. 1996a,b; Lowenthal et al. 1997). All  $u$ -band observations presented in this paper were obtained at the 4.1m Southern Astrophysics Research (SOAR) Telescope located on Cerro Pachon in the Chilean Andes during the 2008B and 2009A semesters. In practice this means that 105 arcs discussed in the paper represent those arcs which had the appropriate  $\alpha$ ,  $\delta$  to be observable during the SOAR observing runs, *and* were discovered prior to the observing runs. The southerly location of SOAR restricts us to arcs with  $\delta \lesssim 20$  degrees, and because our systematic giant arc search is a process that is still on-going, there are many arcs which are now in the sample and have appropriate  $\delta$  to be observable from SOAR but were not known at the time of the  $u$ -band imaging runs.

As discussed in the introduction, it is important to measure the properties for a large, unbiased sample of giant arcs. To that end we note that targets that were observed with SOAR and analyzed here were selected independent of their respective arc radii,  $R_{arc}$ . The arc radius is measured as the mean angular distance on the sky between a giant arc and the center of the foreground cluster lens, where the center is approximated as the center of the BCG. The sample analyzed here includes arcs spanning a large range in arc radius –  $3'' \lesssim R_{arc} \lesssim 55''$  – and the arcs were identified in imaging data that is approximately 1.5 – 2 magnitudes (point source) deeper than those used in Bayliss et al. (2011a), which was restricted to arcs that were visually identified in the SDSS DR7 imaging data.

Some of the giant arcs analyzed in this paper appear in the literature and have published spectroscopic red-

shifts. RCSGA J032727-132609 appears in Wuyts et al. (2010) and Rigby et al. (2011); it is the most spectacular giant arc discovered to date in RCS-2 (and one of the most spectacular systems in the observable universe). RCSGA J152745+065219 is previously published as SGAS J152745+065219 (Koester et al. 2010; Bayliss et al. 2011b), and is located in a region where the RCS-2 and SDSS footprints overlap. SGAS 211119-011429 was first identified as a probably giant arc in Hennawi et al. (2008), and both SGAS 095739+050928 and SGAS 211119-011429 have spectroscopic redshifts published in (Bayliss et al. 2011b). Lastly, the so-called “Cosmic Eye” (Smail et al. 2007) appears in our arc sample, as it is located near on the sky to a massive foreground galaxy cluster, though the arc itself is formed around an elliptical galaxy located behind the galaxy cluster. We include this arc in our sample because it appears in our visual inspection of cluster lines-of-sight, and the foreground cluster contributes significantly to the lensing (Smail et al. 2007). Several other arcs analyzed in this paper have been published as candidate but unconfirmed giant arcs or cluster lenses, including SGAS 084647+044608, SGAS 085429+100819, SGAS 111504+164533, and RCSGA 004827+031114 (Wen et al. 2011).

## 2.2. Follow-up $u$ -band Imaging

All  $u$ -band observations were conducted as part of NOAO programs 2008B-0400 and 2009A-0414 (PI: M. Bayliss) on the 4.1m SOAR Telescope with the SOAR Optical Imager (SOI). SOI is a small mosaic of two  $4096 \times 2048$  pixel CCDs filling a field of view of  $5.25 \times 5.25$  arcmin, with an unbinned pixel scale of  $0.0727''$  pixel $^{-1}$ . Observations of all but one of our targets were taken with the detector binned  $2 \times 2$ , where the remaining target was observed with the detector binned  $4 \times 4$ . Individual exposures varied between 120s and 900s and were dithered to cover the chip gap in the SOI mini-mosaic. Typical total integration times for individual targets range from 240s to 3780s, tuned to provide a minimum imaging depth complementary to the brightness of each visually selected giant arc in the RCS-2  $g$ -band data, with a few systems of particular interest being imaged more deeply (e.g., Wuyts et al. 2010).

Basic image reductions were performed using a combination of custom IDL code and the MSCRED IRAF<sup>2</sup> package. The custom IDL code was employed to remove time-variable detector-based noise structures that appeared in images, as well as for alignment of individual exposures. Flat-fielding, bias correction, and stacking were done using standard MSCRED routines. The resulting stacked  $u$ -band images were calibrated from stars in the SDSS DR7 (Abazajian et al. 2009) that were observed over a range of airmasses:  $1.1 < Z < 1.7$ . For each standard star observation, we solve the following equation:

$$m_u = m_{I,u} + c_0 + c_1 \times (Z - 1) + c_2 \times (m_u - m_g)$$

<sup>2</sup> IRAF (Image Reduction and Analysis Facility) is distributed by the National Optical Astronomy Observatories, which are operated by AURA, Inc., under cooperative agreement with the National Science Foundation.

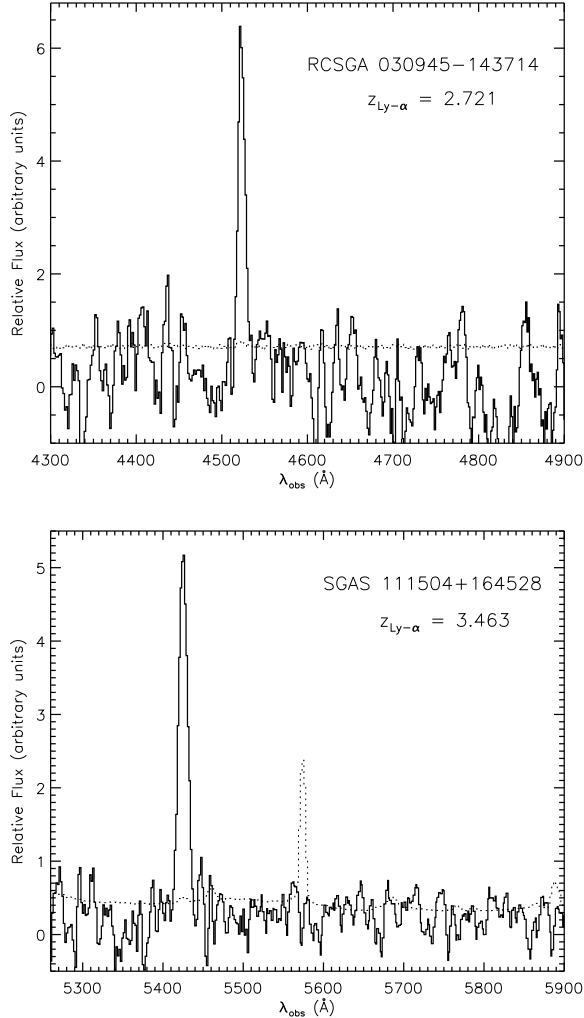


FIG. 2.— Optical spectra with strong Lyman- $\alpha$  emission from two arcs with optical colors measured in this work that identify them as  $z \geq 2.7$  galaxies. The spectroscopic redshifts corroborate the photometric redshift assignment. In each panel the solid histogram represents the measured flux per spectral pixel, and the dotted histogram is the error array. *Top* : Optical spectrum of RCSGA 030945-143714 taken with the Goodman Spectrograph on the SOAR 4.1m telescope. *Bottom* : Optical spectrum of SGAS 111504+164528 taken with DIS on the 3.5m telescope at APO.

where  $m_u$  and  $m_g$  are the true apparent magnitudes of the standard in the  $u$ - and  $g$ -bands, respectively,  $m_{I,u}$  is the measured instrumental magnitude of the standard in a given  $u$ -band observation, and  $Z$  is the airmass of a given observation. By solving the system of equations resulting from all of our standard observations we determine best-fit values for the photometric zero point  $c_0$ , the atmospheric extinction term  $c_1$ , and the photometric color term  $c_2$  for our  $u$ -band observations. The average best-fit values for these terms in 2008B and 2009A observations is  $c_1 = 0.51$  and  $c_2 = 0.02$ . The limiting source of error in the  $u$ -band photometric zero point determination comes from the fundamental uncertainty in the SDSS  $u$ -band calibration;  $u$ -band data is notoriously difficult to calibrate absolutely, a fact that has been well-documented in SDSS photometry<sup>3</sup>. From the

<sup>3</sup> see <http://www.sdss.org/dr7/start/aboutdr7.html>

TABLE 1  
REDSHIFT BINS DEFINITIONS IN COLOR-COLOR SPACE

Redshift Bin	Color Criteria
$2.7 \leq z < 3.5$ :	$g - r \geq -0.35$ , $g - r \leq 1.2$ , $u - g \geq g - r + 1.0$
$1.9 < z < 2.7$ :	$g - r \geq -0.35$ , $g - r \leq 0.2(u - g) + 0.4$ , $u - g \geq g - r + 0.2$ , $u - g < g - r + 1.0$
$1.4 < z < 2.1$ :	$g - r \geq -0.35$ , $g - r \leq 0.2(u - g) + 0.4$ , $u - g \geq g - r - 0.15$ , $u - g < g - r + 0.2$
$1.0 < z < 1.5$ :	$r - z \geq 0.8(g - r) + 0.3$ , $g - r < 1.5$

intrinsic scatter in our standard star observations, and the published photometric characterization for the DR7 (Abazajian et al. 2009), we adopt an upper limit on the uncertainty in our  $u$ -band photometry of  $\pm 0.05$  mags. We also note that there is an established red light leak in the SDSS  $u$  filter that causes slight biases in photometry for red objects, and we therefore restrict stars used in our zero point calibrations to types K and bluer.

### 2.3. Survey Imaging of RCS Giant Arcs (RCSGA) Survey Objects

The RCS-2 survey consists of  $grz$  imaging over approximately  $700 \text{ deg}^2$  taken in queue mode with MegaCam at the 3.6m Canada-France-Hawaii Telescope (CFHT) between 2005 and 2008. Individual RCS-2 pointings have single exposures of 240s, 480s, and 360s in each of the  $grz$  filters, respectively. Because these data are single pointings in each filter, the images contain cosmic rays and chip defects which we remove manually when they occur near one of our giant arcs. The RCS-2 survey data is fully calibrated to the SDSS in all bands, which includes a color term describing the difference between the CFHT MegaCam  $g$ -band and the original SDSS  $g$ -band. The RCS-2 imaging is remarkably uniform in depth and seeing, making it an ideal dataset for homogeneously selecting giant arcs. For further details on the RCS-2 data we refer the reader to Gilbank et al. (2011), which describes the RCS-2 survey data in great detail.

### 2.4. Optical Imaging of Sloan Giant Arcs Survey (SGAS) Objects

The primary  $g$ -band imaging of SGAS systems was obtained at 2.5 – 4m class telescopes over several years (for examples and details of these observations see Hennawi et al. 2008), and it is these data from which the SGAS arcs analyzed here are systematically identified. However, there exists for some of the SGAS giant arcs analyzed in this paper a variety of deeper imaging which we use for photometric measurements where it is available. A subset of the SGAS objects in this paper were also observed in the  $g$ - and  $r$ -bands with the

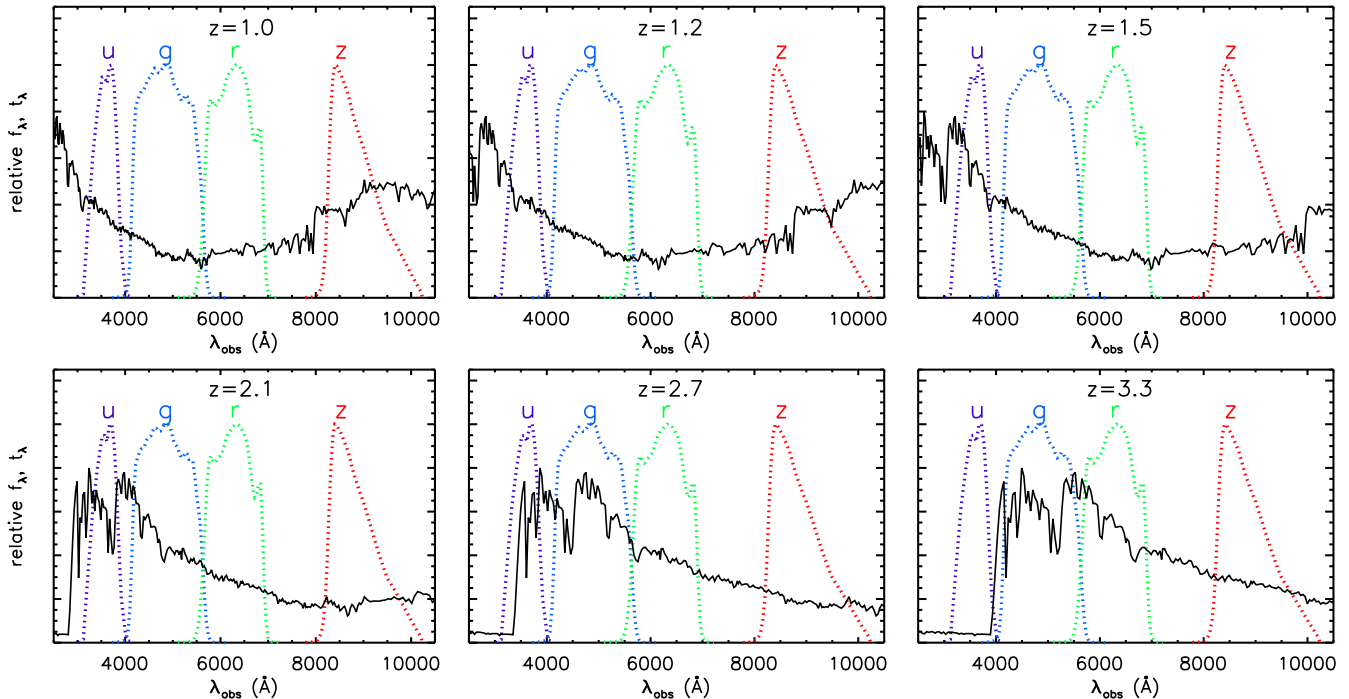


FIG. 3.— Similar to Figure 1 in Adelberger et al. (2004), six panels show a synthetic galaxy spectral energy distribution (SED) at a series of different redshifts, with the *ugrz* filter transmission curves over-plotted as colored dotted lines. The ratio of galaxy fluxes measured in each of the different filters can reliably identify galaxies within different redshift intervals based on the location of strong spectral features, such as the Lyman-limit at  $912\text{\AA}$  (rest-frame), and the Balmer/4000 $\text{\AA}$  break. These strong spectral features appear generically in star-forming galaxies and can be used to assign approximate redshifts for star-forming galaxies without attempting to constrain their specific stellar populations and star-formation histories.

8m Gemini South Telescope with the GMOS instrument (Bayliss et al. 2011b) and/or the 8.2m Subaru Telescope (Oguri et al. 2009, 2011) as a part of a larger program designed to collect extensive follow-up observations for a large subset of the full SGAS sample. We use the best available data for all photometric measurements presented in the paper in order to achieve the highest quality measurements possible. Four of the SGAS objects analyzed here have no deep *r*-band imaging available beyond the publicly available SDSS survey imaging, and so we use these data where necessary. All of the arcs, though confirmed in deeper *g*-band imaging, are sufficiently bright as to be well-detected in the SDSS *r*-band imaging data.

### 2.5. New Spectroscopy of Individual Giant Arcs

In this paper we also present new spectroscopic observations of two arcs in our photometric sample. RCSGA 030945-143714 and RCSGA 030945-143717 were observed with the Goodman Spectrograph (Clemens et al. 2004; Crain et al. 2004) on November 1, 2008 at the end of the first SOAR *u*-band observing run mentioned above (NOAO 2008B-0400). The Goodman Spectrograph is an imaging spectrograph with multi-object capabilities designed to use Volume Phase Holographic (VPH) transmission gratings and optimized for throughput in the wavelength range,  $\sim 3200 - 8000\text{\AA}$ , especially in the blue. We selected the target for spectroscopy from the full *u*-band imaging target list based on the presence of two bright arcs in the field (RCSGA 030945-143714 and RCSGA 030945-143717) that could be observed simultaneously by positioning the slit approximately 40

degrees East of North so as to place both arcs within the slit. The spectrograph was configured with a  $1.03''$  wide longslit mask, the KOSL600 grating, and camera & grating angles of  $20^\circ$  &  $10^\circ$  degrees, respectively. The detector was binned  $2 \times 2$ , resulting in a spatial scale along the slit of  $0.3'' \text{ pix}^{-1}$  and a mean dispersion of  $1.31\text{\AA} \text{ pix}^{-1}$  and a spectral full width at half max (FWHM) of  $4.2\text{\AA}$ . This mode provides a central wavelength of  $5696\text{\AA}$  and wavelength coverage over the range,  $\Delta\lambda = 4200 - 7000\text{\AA}$ .

Science observations of these targets consist of  $4 \times 1800\text{s}$  exposures, with quartz lamp flatfields and HeAr lamp calibration exposures bracketing individual science exposures. The data were reduced, extracted, and stacked using custom IDL scripts that incorporate procedures from the XIDL<sup>4</sup> software package. At the position of RCSGA 030945-143714 along the slit there is a single mildly asymmetric emission line feature is evident in all four individual exposures at  $4523\text{\AA}$ , which we determine to be Lyman- $\alpha$   $\lambda 1216\text{\AA}$  at a redshift,  $z_{\text{arc}} = 2.721$ . Other plausible interpretations for the emission feature (i.e. nebular emission lines at lower redshift) are ruled out by the absence of additional lines in the wavelength range redward of the emission feature ( $\Delta\lambda = 4600 - 7000\text{\AA}$ ). If the emission line was, in fact, O[II]  $\lambda 3727\text{\AA}$  or H- $\beta$   $\lambda 4341\text{\AA}$  then we would expect to also see one or more of H- $\beta$   $\lambda 4862\text{\AA}$ , O[III]  $\lambda 4960, 5007\text{\AA}$  or H- $\alpha$   $\lambda 6563\text{\AA}$  in the wavelength range covered by our observations. We can also note that in our final photometric analysis RCSGA 030945-143714 falls into the appropriate region of

<sup>4</sup> <http://www.ucolick.org/~xavier/IDL/index.html>

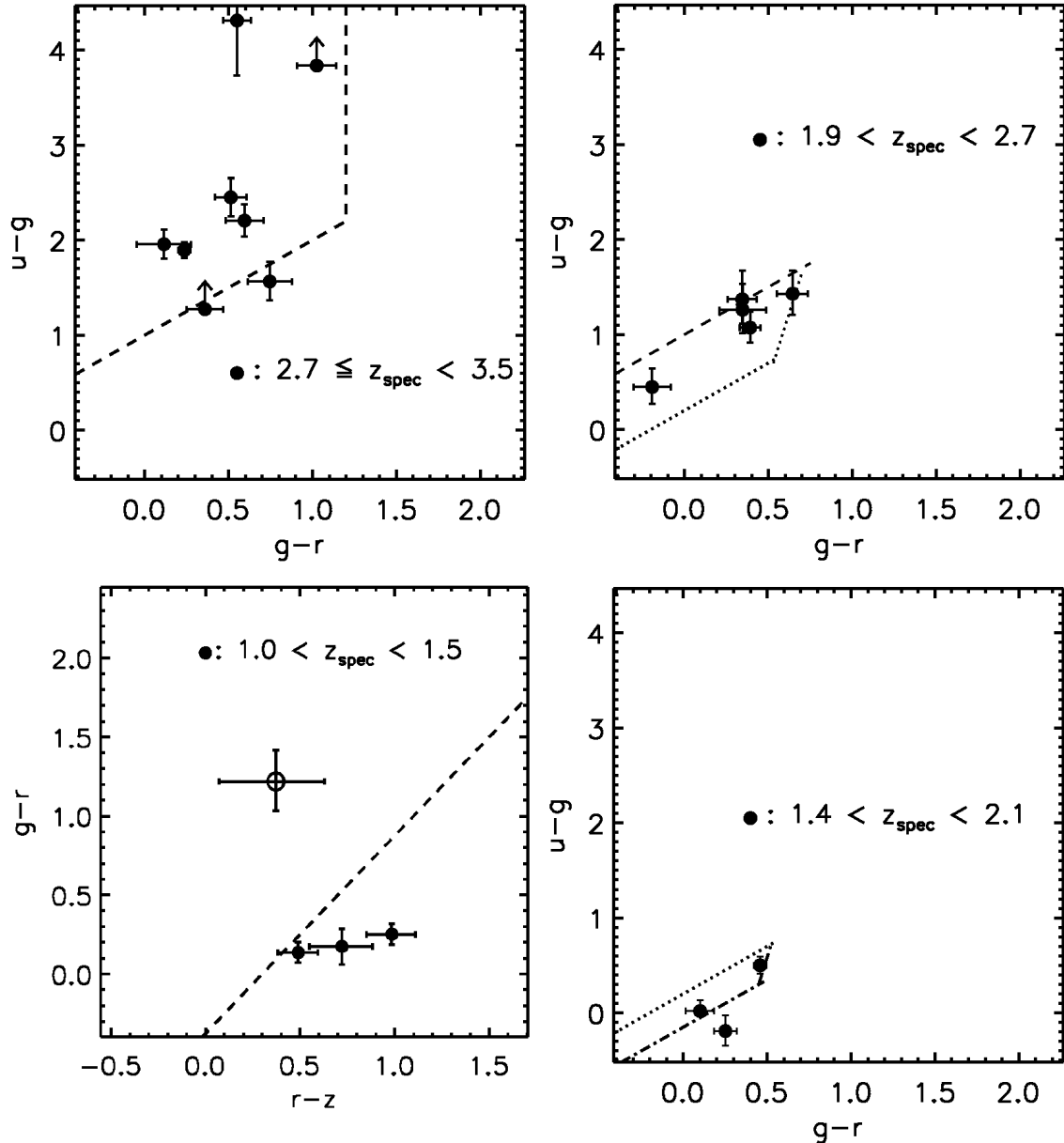


FIG. 4.— Giant arcs with known spectroscopic redshift are plotted in their corresponding color-color space. Each panel plots arcs which match a different redshift bin in color-color space. The bins, beginning in the upper left and proceeding clockwise are,  $2.7 \leq z < 3.5$ ,  $1.4 < z < 2.7$ ,  $1.0 < z < 1.5$ , and  $1.4 < z < 2.1$ . There is some small overlap between some of the neighboring bins, and some arcs are therefore plotted in multiple panels. Arcs with known redshifts agree very well with the corresponding regions in color-color space, with 1/19 lying approximately  $1.8\sigma$  outside of the expected region and several others lying  $1\sigma$  or so outside of the appropriate regions. One arc with a spectroscopic redshift,  $z_{\text{spec}} < 1$  is plotted as an open circle in the lower left panel, and as expected it falls outside of the color-color region corresponding to  $1.0 < z < 1.5$ .

the  $u-g$  vs  $g-r$  space for a galaxy with redshift  $z$ :  $2.7 \leq z < 3.5$ . At the location on the slit corresponding to RCSGA 030945-143717 there is some weak continuum signal spanning the highest-throughput wavelength range for the setup, but nothing sufficient to measure a redshift.

A second giant arc from our sample, SGAS 111504+164528, was also observed with the Dual Imaging Spectrograph (DIS) on the 3.5m Astrophysical Research Consortium (ARC) Telescope at Apache Point Observatory in New Mexico on the night of May 23, 2011. These observations were conducted with DIS in  $1.5''$  longslit mode using the B400/R300 gratings in the

“low-res” configuration. Science exposures consisted of  $2 \times 2400s$ , with quartz lamp flatfields and HeNeAr lamp calibrations bracketing the science exposures. Blue-side spectra have a mean dispersion of  $\delta\lambda = 1.83 \text{ \AA/pix}^{-1}$  and a spectral FWHM of  $5.3 \text{ \AA}$ , and red-side spectra have mean dispersion,  $\delta\lambda = 2.31 \text{ \AA/pix}^{-1}$  and a spectral FWHM of  $6.4 \text{ \AA}$ . The blue and red channels combine to provide full optical wavelength coverage over the range,  $\Delta\lambda = 3800 - 9800 \text{ \AA}$ . These data were reduced and analyzed in the same fashion as the Goodman spectroscopy described above using custom IDL scripts incorporating procedures from the XIDL package.

DIS uses a dichroic splitting optic centered at  $\sim$

TABLE 2  
GIANT ARCS WITH PUBLISHED REDSHIFTS

Giant Arc	$z_{spec}$	Reference
RCSGA 030945-143714	2.719	this work
RCSGA 032727-132609	1.704	Rigby et al. (2011)
RCSGA 213513-010143	3.07	“Cosmic Eye” (Smail et al. 2007)
SGAS 095739+050929	1.820	Bayliss et al. (2011b); Diehl et al. (2009)
SGAS 111504+164528	3.463	this work
SGAS 152745+065219	2.760	Koester et al. (2010); Bayliss et al. (2011b)
SGAS 211119-011432	2.858	Bayliss et al. (2011b)

5500Å, and we observe a single strong emission line in both the blue- and red-side spectra corresponding to the slit position of SGAS 111504+164528, centered at 5425Å. Similar to the case of RCSGA 030945-143714 described above, we conclude that this feature is Lyman- $\alpha$   $\lambda$ 1216Å at a redshift,  $z_{arc} = 3.463$ , based on the lack of other visible emission features over the observed wavelength range  $\Delta\lambda = 3800 - 9800\text{\AA}$ . Similar to the case for RCSGA 030945-143714 above, the SGAS 111504+164528 has  $u - g$  vs  $g - r$  colors that also identify it as a galaxy in the redshift range,  $2.7 \leq z < 3.5$ . Extracted spectra for RCSGA 030945-143714 and SGAS 111504+164528 are shown in Figure 2.

### 3. MEASUREMENTS AND METHODOLOGY

#### 3.1. Optical Selection of Star Forming Galaxies

Historically, Lyman Break Galaxies (LBGs) are selected by examining wide-band photometric data and identifying the redshifted ‘Lyman limit’ continuum break. This strong spectral break appears at 912Å in the rest frame (Steidel et al. 1996a,b; Lowenthal et al. 1997), and moves redward in the rest-frame with increasing redshift – approaching 1216Å – due to Lyman- $\alpha$  forest (Steidel & Sargent 1987; Rauch 1998) absorption by intergalactic neutral hydrogen. Surveys for LBGs are efficient for collecting statistical samples of high-redshift galaxies because it is difficult for galaxies at lower redshifts to mimic the sudden and extreme spectral break of the Lyman Limit. Steidel et al. (2003) published the comprehensive results of a systematic search for  $z \gtrsim 2.7$  galaxies, and this work was extended to probabilistically sort star-forming galaxies into bins at lower redshift intervals by identifying the color-evolution that occurs as additional weaker spectral features redward of the Lyman Limit redshift through a set of optical filters (Steidel et al. 2004; Adelberger et al. 2004). The ratio of galaxy fluxes – or colors – measured in different broadband near-UV, optical, and near-infrared filters can reliably identify galaxies within different redshift intervals based on the location of strong spectral features, such as the Lyman-limit at 912Å (rest-frame), and the Balmer/4000Å break (see Figure 3). These strong spectral features appear generically in star-forming galaxies and can be used to assign approximate redshifts for star-forming galaxies without attempting to constrain their specific stellar populations and star-formation histories. We use this color selection technique and use it to identify the fraction of a complete sample of 105 giant arcs which fall into four broad redshift bins at  $z > 1$  (and by exclusion, giant arcs at  $z < 1$  are also identified).

In order to define photometric dropouts we follow the methodology of Steidel et al. (2003), Steidel et al. (2004), and Adelberger et al. (2004) to define regions in color-color space that correspond to distinct redshift bins. The available photometric data is in a set of filters that are similar to those used in Steidel et al. (2003), Steidel et al. (2004), and Adelberger et al. (2004), with the only significant differences being an  $r$ -band filter with somewhat different characteristics. We use synthetic galaxy spectra from Bruzual & Charlot (2003) with identical stellar age and star formation history properties as are used by Steidel et al. (2003), Steidel et al. (2004), and Adelberger et al. (2004) and step these model spectra through redshift steps of  $\delta z = 0.01$  from  $z = 0.5$  to  $z = 4.0$  and measure the resulting synthetic colors. These simulated galaxy colors as a function of redshift are essentially identical to those appearing in Steidel et al. (2003), Steidel et al. (2004), and Adelberger et al. (2004) with slight differences of  $\sim 0.1 - 0.15$  mags in colors which include the  $r$ -band filter. The final color cut criteria that we apply to our photometry defines four primary redshift bins, all of which are summarized in Table 1.

Arcs that do not satisfy any of the criteria in Table 1 are likely to have redshifts that are either greater than 3.5 or less than 1.0. In principle we might be able to identify very high redshift arcs in our sample (e.g.  $z > 3.5$ ) as  $g$ -band dropouts using logic that is analogous to the original  $u$ -band dropout definitions from Steidel et al. (2003). However, we are limited by the lack of deep imaging redward of the  $r$ -band. In any event, arcs that are very red in  $g - r$  are rare ( $N_{g-r>1.2} = 6$ ), and all of these objects either have  $r - z > 0.9$ , or are detected in  $z$  at less than  $4\sigma$ . This leads us to conclude that arcs which are red in  $g - r$  are likely to be intrinsically red galaxies at  $z < 1$ . That stated, it is still possible that our arc sample contains one or two very high redshift  $g$ -band dropout galaxies, and we account for this possibility in the final uncertainties on our constraints for the giant arc redshift distribution.

#### 3.2. Aperture Photometry of Giant Arcs

We measure four- and three-band photometry for a full sample of 105 giant arcs from the RCSGA and SGAS samples, respectively. All objects have measurements in  $ugr$ , and objects located in the RCS-2 fields have  $z$ -band measurements as well. Photometric measurements are conducted using a custom IDL pipeline that allows us to construct photometric apertures which follow the ridgelines of giant arcs and match the highly variable structures of these objects on the sky, following the proce-

dure used by Wuyts et al. (2010). We draw apertures by manually defining a ridge-line along each giant arc, and convolve the ridge-line with the point spread function (PSF) of each image to create a series of apertures of increasing radius, following isophotes of the convolution. Arcs are typically only resolved along a single axis, because the lensing magnification acts almost exclusively along the tangential direction (relative to the center of the potential of the foreground lens). We therefore measure photometry in each image out to an aperture radius equal to  $2.0 \times \text{FWHM}$ , where the FWHM describes the PSF measured from reference stars in each image. These apertures allow us to measure an equivalent region on the sky for images with different PSFs. All magnitudes are aperture corrected to a radius of  $6''$  using the curve of growth for reference stars in each image.

In cases where the flux for a given arc within its  $2.0 \times \text{FWHM}$  defined aperture is less than  $2\sigma_{app}$ , where  $\sigma_{app}$  is the noise measured within the aperture, we measure a limiting magnitude for that object in that filter. Limiting magnitudes are measured as the magnitude which corresponds to  $2\sigma_{app}$ , and this limiting magnitude is aperture corrected to the same  $6''$  radius as above. Quoted limiting magnitudes are 95% confidence upper limits on the flux from the corresponding arc within its aperture. All photometry is corrected for galactic extinction (Schlegel et al. 1998).

The ridge-line apertures used for this analysis are not necessarily intended to enclose all of the observable flux from each lensed background source. Rather, we draw apertures along the largest contiguous image or arc of each lensed galaxy, and make no attempt to add flux from multiple images/arcs, or faint arc tails that appear to originate or extend away from the same source. Our measurements are conducted with robust color estimates as our primary goal, and our ground-based imaging typically does not have either the depth or image quality to unambiguously identify complete arc families in the same way as can be achieved with adaptive optics or *HST* quality imaging.

We also note that variations in color that can be observed in different lensed images of a single background source may provide a distorted (e.g. cB58; Williams & Lewis 1996) representation of the intrinsic source. That stated, color gradients for star forming galaxies tend to be small – on the order of  $\sim 0.1$  mags (Suh et al. 2010). Color distortions due to magnification gradients across the surface of the lensed sources should therefore be well within the color variations accounted for in the definition of the regions in color-color space, which are intended to apply to star forming galaxies with a variety of colors and there is no reason to expect catastrophic outliers (i.e. giant arcs with apparent colors that differ dramatically from their true intrinsic colors) to be a significant problem for our analysis.

Approximately 1/3rd of the arcs analyzed here are located nearby on the sky to other, presumably foreground, galaxies. For these objects there is light from a projected source, typically the brightest cluster galaxy (BCG) or a cluster member galaxy in the foreground lens, that overlaps with the  $2.0 \times \text{FWHM}$  aperture that we use to measure giant arc arc magnitudes. We have used the publicly available GALFIT package (Peng et al. 2010) to fit Sersic profiles to the nearby galaxies and subtract the

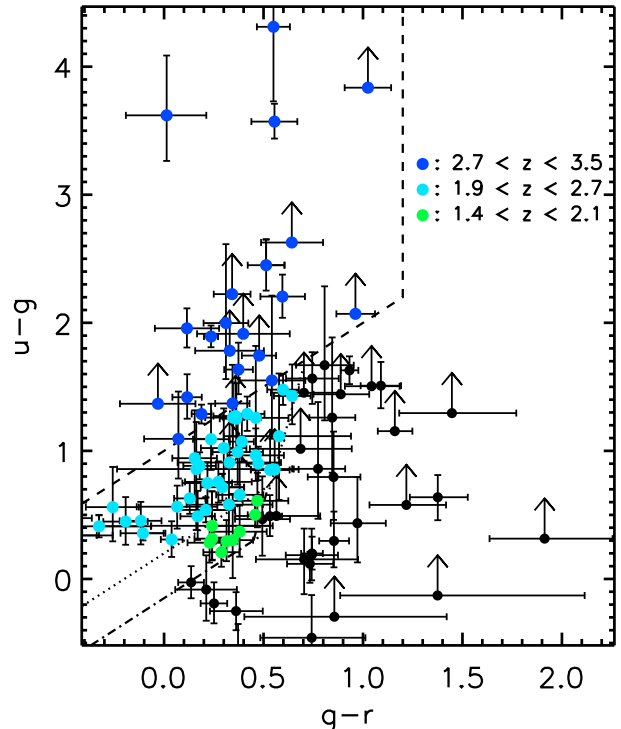


FIG. 5.— Photometric colors,  $u-g$  vs  $g-r$ , for all 105 giant arcs that have  $u$ -band data from SOAR. Three regions in the color-color space are defined by the dashed, dotted, and dot-dashed lines corresponding to redshift ranges,  $2.7 \leq z < 3.5$ ,  $1.9 < z < 2.7$ , and  $1.4 < z < 2.1$ , respectively. Arcs that fall into each respective bin are plotted as blue, cyan, and green points, respectively, while arcs not falling into any of the aforementioned redshift bins are plotted in black; by exclusion these objects have redshifts  $< 1.4$ .

resulting model fluxes. Galaxy light profiles are fit in a filter where the galaxy signal-to-noise (S/N) is high, and that profile is then saved and scaled in brightness to match the galaxy light in the other imaging bands. A single Sersic profile is almost always sufficient to the task for this work because we are generally concerned with subtracting off the extended stellar light profile of BCGs, and we are not concerned with accurately modeling the detailed structure in the BCG core which has no impact on the arc photometry. Occasionally there are very faint intervening galaxies that lack sufficient S/N to achieve a robust GALFIT model, and we remove these galaxies by manually masking the galaxy pixels.

### 3.3. Verification of Color-Based Redshift Assignment

We can directly test the validity of applying the Steidel et al. (2003), Steidel et al. (2004), and Adelberger et al. (2004) color criteria for rough redshift assignment to our sample of giant arcs by comparing spectroscopic redshifts for individual giant arcs against their color-color space redshift designation. All photometric measurements were made blind to any prior redshift knowledge for our giant arc sample, and after the fact we identify 19 giant arcs in our sample that have known, high-confidence spectroscopic redshifts. Five of these giant arc redshifts are in the literature, while the remaining 14 are the result of new observations. Two of

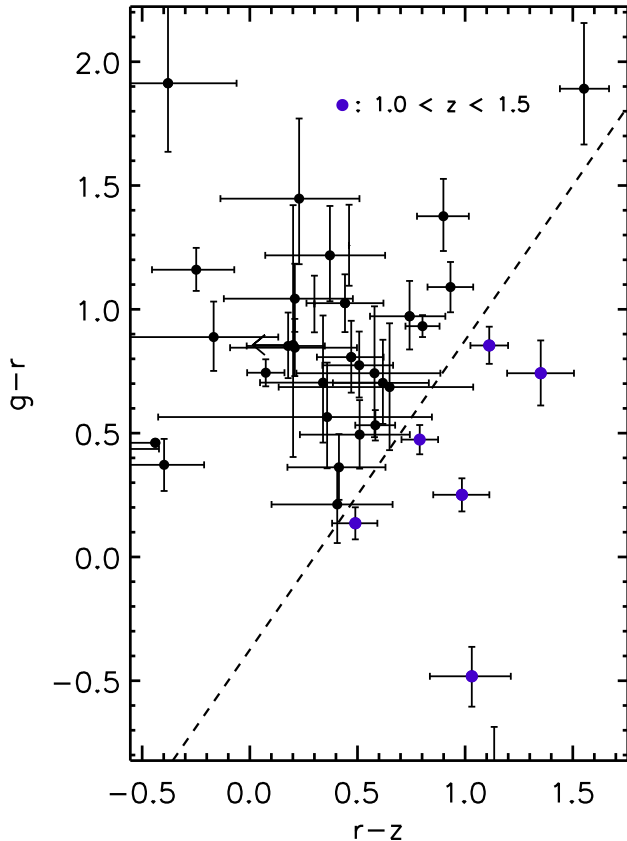


FIG. 6.— Colors,  $g-r$  vs  $r-z$ , for 96 arcs discovered in the RCS-2 survey area. The dashed line indicates the division in the color-color space that identifies typical star forming galaxies at  $1.0 < z < 1.5$  (these galaxies are located to the right/below the dashed line). Arcs satisfying this criteria are plotted in purple, while other arcs are plotted in black. Several arcs, including many of those with marginal or poor  $z$ -band photometry fall outside of the color-color region shown in the plot.

these new redshifts are presented here (see Section 2.5), and the remaining 13 will appear in forthcoming publications: one in M. D. Gladders et al. 2011, in preparation and 12 in M. Carrasco et al. 2012, in preparation). The authors of these papers have generously granted us access to the unpublished spectroscopic redshifts for the purpose of verifying the color-color redshift designation method used in this paper. The seven giant arcs with public redshift information (five published plus two new arcs presented here) are summarized in Table 2.

In order to verify the success of the color-color based methodology when applied to our giant arc sample, we populate the relevant color-color spaces with measured colors for arcs of known redshift in our sample and compare their location to the regions defined based on the methods first published in Steidel et al. (2003), Steidel et al. (2004), and Adelberger et al. (2004). The resulting  $u-g$  vs  $g-r$  and  $g-r$  vs  $r-z$  plots are shown in Figure 4, and provide excellent validation of the use of cuts in color-color space as a tool for estimating the redshifts of our giant arc sample. We can perform an additional sanity check by comparing the redshift bin assignments for the giant arcs against photometric red-

TABLE 3  
FRACTION OF ARCS SATISFYING  
DIFFERENT COLOR CRITERIA

Redshift Bin	Fraction of Arcs
$2.7 \leq z_{arc}$	$0.21^{+0.04}_{-0.02}$
$1.9 < z_{arc} < 2.7$	$0.33^{+0.03}_{-0.03}$
$1.4 < z_{arc} < 2.1$	$0.09^{+0.04}_{-0.02}$
$1.0 < z_{arc} < 1.5$	$0.08^{+0.04}_{-0.02}$
$z_{arc} < 1.0^a$	$0.29^{+0.03}_{-0.05}$

<sup>a</sup> Fraction of arcs with  $z < 1.0$  is measured by exclusion, i.e. giant arcs with colors not meeting the other criteria covering the redshift range  $1.0 < z \lesssim 3.5$ .

shifts for the foreground cluster lenses that are measured as a part of the red-sequence cluster finding algorithm. Indeed, we find that the giant arcs which are sorted into the  $z \leq 1$  redshift bin are not formed by clusters that have  $z_{phot} \gtrsim 0.8$ , which is encouraging given that the geometry of such systems makes the occurrence of strong lensing difficult at best (and non-physical at worst). A broad examination of the relationship between  $z_{lens}/z_{arc}$  pairs yields no significant correlation.

#### 3.4. Redshift Constraints On 105 Giant Arcs

Giant arc  $u-g$  vs  $g-r$  and  $g-r$  vs  $r-z$  colors are shown in Figure 5 and Figure 6, respectively. Individual giant arc color measurements are color-coded in the figures according to the redshift bins that they fall into. The  $g-r$  vs  $r-z$  color space in Figure 6 is populated using only RCSGA survey objects, because we lack  $z$ -band imaging of sufficient depth for our SGAS arcs. RCSGA arcs, however, comprise  $> 90\%$  of our full giant arc sample, and we can also note that seven of the nine SGAS arcs fall into redshift bins based on their  $u-g$  vs  $g-r$  colors, so that the lack of  $z$ -band data for the SGAS sample only prevents us from assigning two systems to one of the  $z < 1.0$  or  $1.0 < z < 1.5$  bins, which has a negligible affect on our ability to characterize the redshift distribution of the sample as a whole.

The resulting constraints on the fraction of arcs falling within each redshift bin are shown in Table 3. We estimate the errors on the fractions of giant arcs meeting various redshift criteria by generating  $10^4$  Monte Carlo realizations of our data, where each realization is a simulated dataset that is generated by assuming that each photometric measurement is gaussian distributed about the measured value, with standard deviations equal to the  $1\sigma$  errors on the measurements. Some photometric measurements have asymmetric errors, and for these cases the simulated data accounts for the asymmetry in the errors. We make no attempt to recover a total probability distribution,  $dp_{arc}/dz$ , because doing so requires detailed knowledge of the probability distribution of redshifts within each bin in color-color space, which we do not have. Instead we simply report the total cumulative fraction of giant arcs which have redshifts,  $z_{arc}$ , greater than various discrete cuts. The resulting cumulative redshift fractions are  $71^{+5}_{-4}\%$  at  $z \geq 1.0$ ,  $64^{+6}_{-4}\%$  at  $z \geq 1.4$ ,  $56^{+5}_{-4}\%$  at  $z \geq 1.9$ , and  $21^{+4}_{-2}\%$  at  $z \geq 2.7$ . The fraction of arcs with  $z \geq 1.4$  and  $z \geq 1.9$  requires making some

assumptions about the probability distribution within each redshift bin, because some of the neighboring bins have regions of overlap in redshift. For example, in order to compute the fraction of giant arcs with  $z \geq 1.4$ , we first account for all arcs that have colors identifying them as galaxies at  $2.7 \leq z_{arc} < 3.5$ ,  $1.9 < z_{arc} < 2.7$ , and  $1.4 < z_{arc} < 2.1$ . We then must estimate the fraction of arcs within the redshift range,  $1.0 < z_{arc} < 1.5$ , that we expect to have  $z_{arc} > 1.4$ . For these reported values we assume that giant arc redshifts within a bin are roughly gaussian distributed within that bin with a standard deviation that is based on the results of spectroscopic follow-up for galaxies falling within these same color-based redshift bins in Adelberger et al. (2004).

### 3.5. Giant Arc Linear Brightness Measurements

In addition to the optical colors of our giant arc sample, we also measure the linear brightnesses for each arc in the  $g$ - and  $r$ -bands. The linear brightness is computed for a given arc by dividing the total aperture magnitude for each arc by the length of the aperture, in arcseconds. This quantity is a very useful observable for giant arcs with ground-based imaging data, where the arcs are typically unresolved in the radial direction (with respect to the center of the foreground lensing potential). So long as an arc is resolved along the tangential direction (again, with respect to the center of the foreground lensing potential) – a condition that is essentially always satisfied – then the linear brightness is an observable that can be extracted from the data. The linear brightness has the appealing property of being independent of the PSF of the seeing of a particular image, and it is an observable quantity that can be easily produced for simulated giant arcs by convolving simulated imaging data with a smoothing kernel that is chosen to match the image quality of real imaging data.

Figure 7 shows the distribution of both integrated and linear magnitudes for our complete arc sample in both the  $g$ - and  $r$ -bands. The measured distribution of linear magnitudes for a statistical sample of giant arcs is an observable which, like the arc redshift distribution, informs predictions of giant arc statistics by providing direct constraints on the photometric properties of simulated giant arcs. Specifically, the linear magnitudes of arcs should depend on some combination of two factors: 1) the typical magnifications for the lens-source systems, and 2) the intrinsic surface brightness function of the lensed background sources. Simulated arc samples must be able to reproduce the observed linear magnitude distribution in order to ensure that they are providing a robust simulation of the physical universe.

## 4. DISCUSSION AND SUMMARY

### 4.1. A Census of Physical Factors Relevant to Predictions for Giant Arcs

As we summarized in the Introduction, there has been no shortage of ideas for physical effects which, if unaccounted for in cosmological simulations, can explain varying degrees of discord between giant arc statistics predictions and observations. One such factor that has been directly addressed in the literature is the impact that baryons can have on the strong lensing cross-section for galaxy clusters (Puchwein et al. 2005; Rozo et al.

2008; Wambsganss et al. 2008). Rozo et al. (2008) find that the inclusion of baryonic cooling results in significant steepening of the central density profile relative to what is seen in dark matter only simulations and estimate that these processes can increase giant arc abundances by as much as a factor of a few, and Wambsganss et al. (2008) find more modest increases of  $\sim 25\%$ . However, the real-world impact is very likely to be smaller than measured by these authors due to the well-established “over-cooling” problem in simulations (e.g., Balogh et al. 2001). In fact, more recent studies of strong lensing efficiencies in simulations that include gas physics find that the inclusion of feedback processes serves to mitigate the increase in strong lensing efficiency that result from including baryonic cooling physics (Mead et al. 2010).

One key property of massive halos that does have a large impact on their ensemble lensing efficiencies is the triaxiality of their matter distributions. Halos identified in dark matter simulations are known to have triaxial shapes (Kasun & Evrard 2005; Allgood et al. 2006), and the triaxiality can cause large orientation-dependent variations in the strong lensing cross-section for individual halos (Oguri et al. 2003; Dalal et al. 2004; Hennawi et al. 2007; Meneghetti et al. 2010). This effect should be well-accounted for in predictions of giant arc counts using large volume simulations (e.g., Hennawi et al. 2007; Meneghetti et al. 2010). We must also point out, however, that the triaxiality of the matter distribution in the cores of clusters in simulations is sensitive to the presence/absence of gas physics. Baryonic cooling processes cause the shape of the density profile in cluster cores to become much less triaxial than in pure dark matter simulations (Kazantzidis et al. 2004; Rozo et al. 2008), which could mitigate the importance of triaxiality and the magnitude of an orientation bias.

Simulations that account for the presence of baryonic matter by populating dark matter simulated halos with evolved mock galaxies may also be able to increase the number of expected giant arcs, but different studies claim varying increases in the efficiency of giant arc production. Dark matter only simulations with galaxies “painted on” after the fact cannot account for the detailed effects that baryons have on the shape and steepness of the matter density profile, but the inclusion of a large concentration of baryonic matter in the cores of simulated halos does produce an increase in the strong lensing cross-section. The size of the impact that painted on galaxies have on giant arc counts is claimed to be as small as  $\lesssim 25\%$  (Flores et al. 2000; Meneghetti et al. 2000, 2003), and as large as a factor of 2 (Hilbert et al. 2008). Though the precise magnitude of the effect of including galaxies in ray-tracing simulations of giant arcs varies in the literature, there is no evidence that it approaches the factors of  $\sim 10$  necessary to account for the difference between current arc counts and the predictions by Bartelmann et al. (1998).

The impact of dark matter substructure in cluster-scale halos has also been suggested as a potentially important factor (Flores et al. 2000; Meneghetti et al. 2000, 2003), but work done to quantify the contribution of substructure to lensing efficiency suggests that it is negligible (Hennawi et al. 2007). Other recent work indicates that the efficiency for giant arc production of individual clusters seems to be in good agreement when comparing the

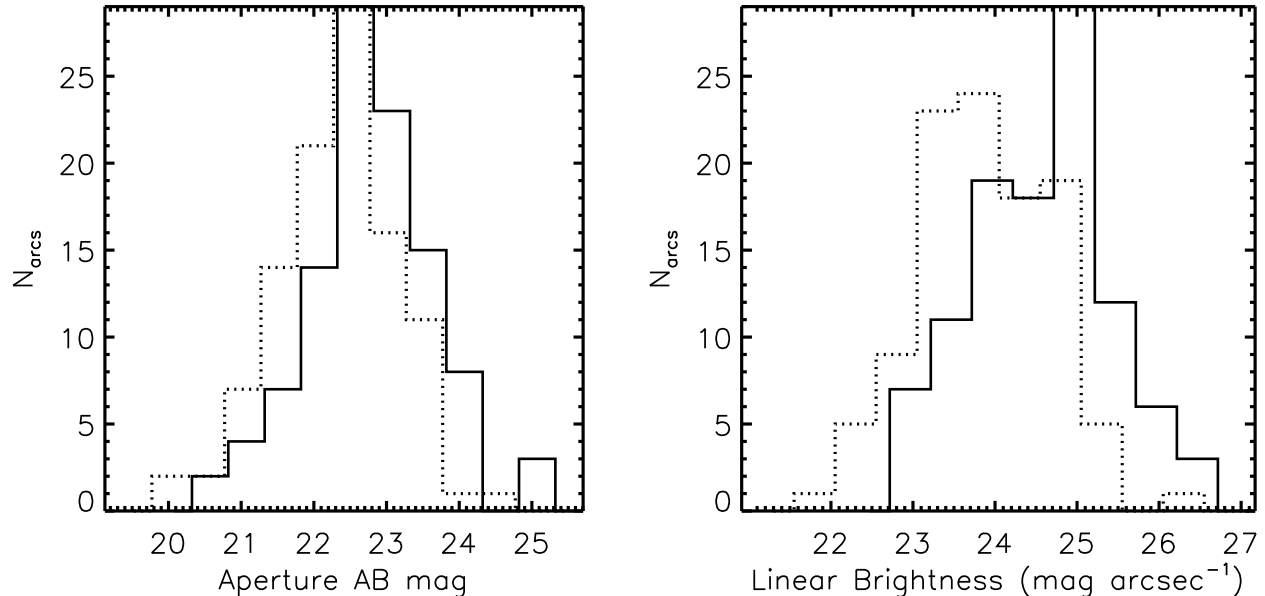


FIG. 7.— Distribution of magnitudes for all giant arcs presented in this paper. *Left*: Integrated magnitudes for all arcs; the solid line histogram shows  $g$ -band magnitudes, and the dashed line histogram shows  $r$ -band magnitudes. *Right*: Linear magnitudes for the entire arc sample, where the solid and dashed line histograms again correspond to the  $g$ - and  $r$ -band, respectively.

number of giant arcs produced *per cluster* in *HST* imaging of X-ray selected cluster samples against mock images created from ray tracing modern simulated massive clusters (Horesh et al. 2005, 2011).

Horesh et al. (2011) use the Millennium Simulation (Springel et al. 2005) with galaxies included via a semi-analytic prescription, so that the galaxy contribution to the lensing efficiency of individual clusters is accounted for. Notably, this work *does not* address the question of the overall abundance of giant arcs – e.g. giant arc counts over a well-quantified fraction of the sky imaged to a well-defined depth – but it does isolate the question of whether there is a systematic discrepancy between the strong lensing efficiencies of individual simulated vs. real clusters. As summarized above, a study of the global increase in giant arc counts in the Millennium Simulation, including galaxies, suggests a factor of 2 increase over the earlier work of Bartelmann et al. (1998). The Horesh et al. (2011) result therefore imply that the apparent discrepancy between the real and predicted giant arc abundances is primarily due to factors other than those having to do with the internal structure of galaxy clusters (e.g., contributions to the project surface mass density from abnormally high concentrations, substructure, or cluster galaxies).

With clear motivation now to focus on factors beyond the internal properties of simulated clusters, there are several potential effects on which to focus our attention. Two additional ideas that have been explored in the literature are the contribution to cluster lensing efficiency from large scale structure (e.g. filaments and uncorrelated halos) along the line of sight looking out toward massive clusters (Wambsganss et al. 2005; Hilbert et al. 2007; Puchwein & Hilbert 2009), and short timescale increases in the lensing cross-sections of individual clusters due to major mergers (Torri et al. 2004). Stud-

ies using the Millennium Simulation conclude that the resulting increase in the strong lensing efficiency from these unrelated, projected density effects is in the  $\sim 30\%$  range, and are therefore not sufficient to significantly ease the tension between giant counts observed and predicted. Observational tests looking for projected line-of-sight structure toward strong lenses (Faure et al. 2009; Fassnacht et al. 2011) find no evidence of an increase in the amount of uncorrelated structure near lenses vs. the field, in agreement with the simulation-based results.

With regard to mergers, Torri et al. (2004) find an increase of nearly an order of magnitude in an individual cluster’s strong lensing cross-section during a merger, the short timescale of the boosted cross-section and the infrequency of major mergers in cluster-scale halos make it difficult for mergers to contribute substantially to the integrated efficiency of galaxy cluster strong lensing (Hennawi et al. 2007). Fedeli et al. (2006) conclude that accounting for mergers in simulations can nearly double the strong lensing optical depth for a subset of lenses – those at  $z \geq 0.5$ . However, a large fraction of cluster lenses lie at  $z < 0.5$ , thus reducing the total magnitude of merger effects on simulated giant arc samples.

Having accounted for an exhaustive set of physical factors that could increase giant arc counts by making simulated clusters into better strong lenses, we are left with one hypothesis that has nothing at all to do with the cluster lens population. Hamana & Futamase (1997) first argued that giant arc statistics depend sensitively on any evolution of the galaxy luminosity function at high redshift, and Oguri et al. (2003) identify the uncertainty in the galaxy luminosity function at high redshift as a factor that can significantly impact predictions for giant arcs based on their semi-analytic models. This effect was quantified in simulations by placing background sources at a series of different redshift planes and com-

puting the integrated strong lensing cross section for a simulated cosmological volume as a function of source redshift (Dalal et al. 2004; Wambsganss et al. 2004).

Interestingly, Wambsganss et al. (2004) are able to approximately reproduce the Bartelmann et al. (1998) predictions by using a background galaxy population placed entirely at  $z_s = 1$ , but when background galaxies are placed at  $z_s = 1.5$  they recover a factor of  $\sim 10$  increase in the number of predicted giant arcs, and a factor of  $\sim 20$  increase for sources at  $z_s = 2$ . Dalal et al. (2004) also identify a significant increase in the total strong lensing cross-section with increasing source redshift, but measure the increased cross-section at higher source redshift to be a factor of  $\sim 3$  smaller than Wambsganss et al. (2004). Simulations which evaluate lensing efficiency with all sources placed at a single source plane are not physically realistic, but the work by Wambsganss et al. (2004) and Dalal et al. (2004) emphasizes the importance of understanding the distribution of source redshifts of background galaxies available to be strongly lensed by foreground galaxy clusters.

#### 4.2. These Results In the Context of Other Work

There is strong evidence that the total strong lensing cross-section for galaxy clusters can easily be increased by as much as a factor of at least  $\sim 7 - 10$  if a majority of the sources lensed into arcs reside at  $z \gtrsim 2$ . Our results analyzing the optical colors for a large, well-selected sample of 105 giant arcs provide a measurement of the distribution of redshifts for sources which are lensed into arcs, with  $71_{-4}^{+5}$  % at  $z \geq 1.0$ ,  $64_{-4}^{+6}$  % at  $z \geq 1.4$ ,  $56_{-4}^{+5}$  % at  $z \geq 1.9$ , and  $21_{-2}^{+4}$  % at  $z \geq 2.7$ . The inferred median redshift here is approximately  $\bar{z}_s = 2.0$ , which is consistent with the median redshift of 1.82 determined from a much smaller sample in Bayliss et al. (2011a). Also encouragingly, the fraction of giant arcs measured at  $z > [1.0, 1.4, 1.9]$  in this paper and in Bayliss et al. (2011a) are consistent to within the statistical errors of the two measured redshift distributions. As a caveat to the sorting of arcs into precise redshift bins, we point out that the assumptions that go into defining regions in color space that associate with specific redshift ranges are likely to be much more robust in some cases than others. Specifically, the Lyman- $\alpha$  forest and the Lyman-limit break moving through the  $u$ -band at  $z \gtrsim 1.9$  will strongly affect the  $u-g$  color of any galaxy regardless of the shape of its spectral energy distribution (SED). Color criteria at  $z \lesssim 1.9$ , however, rely more heavily on the robustness of the assumptions made about the properties of the stellar populations within the observed galaxies.

With robust measurements of the giant arc redshift distribution for two samples of giant arcs, it is also important to confirm that the measured distributions are sensible in the context of other observations of high redshift galaxy populations. Bayliss et al. (2011a) test the redshift distribution of 28 bright giant arcs against simple physical models based on results from strong lensing simulations and galaxy catalogs from the COSMOS survey (Ilbert et al. 2009) and find good agreement with the observed redshift distribution. The form of the model redshift distribution is,

$$\frac{dp_{\text{arc}}}{dz_s} = \frac{\sigma_{\text{arc}} \frac{dn}{dz_s}}{\int dz_s \sigma_{\text{arc}} \frac{dn}{dz_s}},$$

where the model uses a normalized strong lensing cross-section from Fedeli et al. (2010) evaluated at a single source plane,  $z_s = 2$ , and we solve for the giant arc cross-section at different source redshifts by assuming a universal density profile that is described by a power-law slope,  $\alpha$ , in the regions where strong lensing is observed. The number density of background galaxies as a function of redshift can be computed from the COSMOS catalogs for a given limiting magnitude and an estimate of the average magnification factor. We do not have good constraints on the average magnification of these sources, and the literature is not unanimous on the precise value of the slope of the density profile,  $\alpha$ , in the cores of clusters. However, by testing models that sample a range of reasonable values for these two parameters ( $-1.7 < \alpha < -1.3$ ,  $26 < g_{lim} < 24$ ) we can produce synthetic redshift distributions that are in good agreement with the data (Bayliss et al. 2011a). Though the broad bins that we define in this paper limit our ability to perform the same statistical comparisons that are used in Bayliss et al. (2011a), we can compare the fractions of arcs above various thresholds in the models and in our color-based redshift constraints and find good agreement. Because the sample analyzed in this paper was identified in imaging that is approximately 2 magnitudes deeper than that used in Bayliss et al. (2011a), the fact that both redshift distributions can be well-described by the same simple physical models has an interesting implication; the primary difference between the brightest arcs selected from shallower imaging vs somewhat fainter arcs found in deeper imaging is that the brighter arcs are typically the cases with the most extreme magnifications.

#### 4.3. Implications for Giant Arc Statistics

With the giant arc redshift distribution now constrained in this paper, it is possible to calculate the approximate increase in the total cross-section for arc production compared to published predictions. We estimate the relative cross-section for different background source redshift distributions using Figure 1 in Wambsganss et al. (2004), which provides a measurement of the strong lensing cross-section as a function of source redshift. The total cross-section for our measured redshift distribution is simply the integrated cross-sections from Wambsganss et al. (2004) Figure 1, weighted by the fraction of giant arcs determined to be within different redshift bins. The uncertainty in this determination is propagated from the color-based redshift identification, estimated by varying the weights in accordance with our measured uncertainties in the fraction of giant arcs located within each redshift bin (see Table 3).

The resulting total increase in the efficiency for giant arc production, normalized to the Bartelmann et al. (1998) result with lensed sources at  $z_s = 1$ , is  $\sigma_{SL}/\sigma_{SL,z=1} = 10.3_{-0.6}^{+1.1}$ . The uncertainty reported in this measurement does not incorporate an attempt to account for published evidence that the magnitude of the effect is smaller than Wambsganss et al. (2004) claim (Dalal et al. 2004; Li et al. 2005; Fedeli et al. 2006), but it is clear that the high-redshift nature of the lensed sources is a significant factor to be accounted for in predictions of giant arc abundances. We can compare our new estimate of  $\sigma_{SL}/\sigma_{SL,z=1}$  to the same value es-

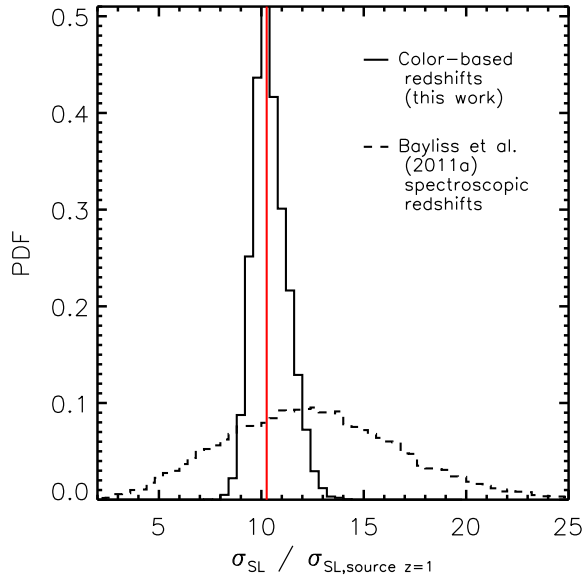


FIG. 8.— The probability distribution for the estimated increase in the total cross-section for the production of gravitationally lensed arcs with length-to-width ratios  $\gtrsim 5$ , relative to the predictions of Bartelmann et al. (1998). Estimates are made from the redshift distribution derived in this paper using color-based redshift assignments (solid line), as well as the redshift distribution reported in Bayliss et al. (2011a) (dashed line). The two estimates of the increase in giant arc cross-section have nearly identical expectation values of  $\sigma_{SL}/\sigma_{SL,z=1} = 10.3$  – indicated by the vertical red line – but the much larger sample used in this work vastly improve the precision of the estimate.

estimated using the spectroscopic redshift distribution of Bayliss et al. (2011a),  $\sigma_{SL}/\sigma_{SL,z=1} = 11^{+5}_{-3}$  (Figure 8). The improved constraints on the arc redshift distribution using a sample of 105 – along with the fact that four of the 28 arcs analyzed in Bayliss et al. (2011a) had only very broad redshift constraints spanning a range in  $\Delta z = 1.8$  – provides a much tighter estimate of the increase that we should expect in giant arc counts when using an empirically calibrated redshift distribution, relative to the simple  $z_s = 1$  used in Bartelmann et al. (1998). Modern efforts to simulate giant arc counts can incorporate the empirically determined giant arc redshift and brightness measurements that we provide in this work, and thus produce refined predictions for giant arc statistics.

We have established that incorporating a background source population into future efforts to predict giant arc counts should increase the number of predicted arcs by as much as a factor of  $\sim 10$  beyond the results of Bartelmann et al. (1998), and thereby diffuse the tension between observations and prediction for arc counts. However, we have yet to discuss an important detail regarding most published work in which giant arcs are produced by ray-tracing simulations. Specifically, most simulations run in the past  $\sim 10 - 15$  years were run in cosmologies with a value for the normalization of the matter power spectrum,  $\sigma_8$ , that is higher – typically  $\sigma_8 = 0.9 - 0.95$  – than the value that is preferred by current observational constraints of  $\sigma_8 \sim 0.81 \pm 0.03$  (Komatsu et al. 2011; Larson et al. 2011). The precise value of  $\sigma_8$  used in simulations is of particular impor-

tance for predictions of giant arc statistics because the high-end tail of the mass function varies sensitively with  $\sigma_8$ .

The quantitative impact of  $\sigma_8 \sim 0.81$  on predictions of giant arc counts has been studied with N-body (Li et al. 2006) and semi-analytic techniques (Fedeli et al. 2008), and both confirm the intuitive expectation that lower values of  $\sigma_8$  result in significantly lower giant arc abundances. The difference between a cosmology with  $\sigma_8 = 0.9$  vs  $\sigma_8 = 0.74$  is found to be a factor of  $\sim 6$  in simulations (Li et al. 2006), and semi-analytic modeling by Fedeli et al. (2008) suggests that  $\sigma_8 \sim 0.8$  under-predicts giant arc counts by an order of magnitude even after attempting to account for factors such as mergers and cluster substructure.

The Fedeli et al. (2008) models do not account for contributions from galaxies embedded in cluster potentials, and use a background source description that is based on somewhat out-dated observations using the Hubble Deep Field (Casertano et al. 2000) that are subject to large cosmic variance uncertainties (Hennawi et al. 2007), but the fact that an order of magnitude discrepancy persists in this work is clear motivation for the pursuit of modern simulations to better-characterize the expected giant arc abundance. The machinery is in place to produce these predictions in such a way that any persistent under-abundance of giant arcs in theory can be reasonably interpreted as evidence for real tension between the growth of structure in  $\Lambda$ CDM – in the form of the abundance of the most massive clusters – and the integrated strong lensing properties observed in the universe. New, large giant arc samples are in the process of being identified from wide-field imaging survey data, and will soon be available in the literature (M. D. Gladders et al. 2011, in preparation; M. B. Bayliss et al. 2012, in preparation). These forthcoming samples will provide observational constraints that match the fidelity of the next generation of improved predictions, and set the stage for a definitive test of giant arc statistics.

#### 4.4. Other Applications for A Catalog of Lensed Galaxies At $z > 2$

The current literature contains a modest sample of extremely bright strongly lensed galaxies (e.g., Yee et al. 1996; Smail et al. 2007; Koester et al. 2010; Wuyts et al. 2010), some of which have been the target of detailed multi-wavelength follow-up studies (Finkelstein et al. 2009; Siana et al. 2009; Quider et al. 2010). Studies of individual galaxies at high redshift are limited by the intrinsic faintness of the sources – especially where high fidelity observations of typical  $\sim L^*$  galaxies are concerned. However, because faint galaxies ( $L \lesssim L^*$ ) are far more numerous than bright ones and therefore more likely to lie on the caustic of foreground lensing clusters, we should expect most giant arcs to be intrinsically sub- $L^*$  galaxies. It follows then that strongly lensed galaxies are ideal targets for studying the properties of *typical* high- $z$  galaxies at S/N that is unavailable in studies of galaxies in the field. By analyzing the optical broadband colors of 105 arcs, we have shown that approximately half of all giant arcs formed around galaxy clusters can be expected to lie at  $z \gtrsim 2$ . Forthcoming large catalogs of hundreds of galaxies that are strongly lensed by clusters should therefore provide of order hundreds of strongly lensed

high-redshift sources that will be accessible for detailed individual study with the instrumentation available on 8 – 10m class telescopes.

#### 4.5. Summary

We have measured *ugr* magnitudes for a sample of 105 giant arcs, and *z*-band magnitudes for 96/105 of the same sample. The giant arc sample was identified in a systematic search of uniform depth *g*-band imaging data, and constitutes a representative subsample of two forthcoming large samples of giant arcs that are currently being identified in search of well-characterized cosmological search volumes. We then sort all 105 arcs into five redshift bins based on well-established broadband color criteria, and thereby constraint the underlying redshift distribution of giant arcs identified with our selection method. The data indicate that  $z_s = 2.0 \pm 0.1$  is the typical redshift for these giant arcs, which agrees remarkably well with the redshift distribution measured from spectroscopic observations of a much smaller sample ( $N = 28$ ) giant arcs that were identified in much shallower imaging data. By establishing that approximately half

of all bright giant arcs are galaxies at  $z \gtrsim 2$  we provide strong evidence for an easing of the tension between observations and predictions of the total abundance of giant arcs on the sky.

Support for this work comes in part from the Illinois Space Grant Consortium in the form of a graduate fellowship. I want to first give my sincere thanks the SOAR observing and support staff for their help in obtaining the observations that drove this paper. I also want to thank Michael Gladders, David Gilbank and Howard Yee for their work on RCS-2, Eva Wuyts for helpful discussions about giant arc photometry and SSP galaxy models, Felipe Barrientos and Mauricio Carrasco for graciously sharing unpublished spectroscopic redshifts, and Brad Holden for helpful discussion that expanded the scope of this work. I also want to thank my thesis committee members – Stephen Kent, Andrey Kravtsov and Richard Kron – for their helpful comments. Lastly, I want thank Michael Gladders for his dedication and mentoring over the past four years.

#### REFERENCES

- Abazajian, K. N., et al. 2009, *ApJS*, 182, 543  
 Adelberger, K. L., Steidel, C. C., Shapley, A. E., Hunt, M. P., Erb, D. K., Reddy, N. A., & Pettini, M. 2004, *ApJ*, 607, 226  
 Allgood, B., Flores, R. A., Primack, J. R., Kravtsov, A. V., Wechsler, R. H., Faltenbacher, A., & Bullock, J. S. 2006, *MNRAS*, 367, 1781  
 Balogh, M. L., Pearce, F. R., Bower, R. G., & Kay, S. T. 2001, *MNRAS*, 326, 1228  
 Bartelmann, M., Huss, A., Colberg, J. M., Jenkins, A., & Pearce, F. R. 1998, *A&A*, 330, 1  
 Bayliss, M. B., Gladders, M. D., Oguri, M., Hennawi, J. F., Sharon, K., Koester, B. P., & Dahle, H. 2011a, *ApJ*, 727, L26+  
 Bayliss, M. B., Hennawi, J. F., Gladders, M. D., Koester, B. P., Sharon, K., Dahle, H., & Oguri, M. 2011b, *ApJS*, 193, 8  
 Broadhurst, T. J., Taylor, A. N., & Peacock, J. A. 1995, *ApJ*, 438, 49  
 Bruzual, G., & Charlot, S. 2003, *MNRAS*, 344, 1000  
 Casertano, S., et al. 2000, *AJ*, 120, 2747  
 Clemens, J. C., Crain, J. A., & Anderson, R. 2004, in Presented at the Society of Photo-Optical Instrumentation Engineers (SPIE) Conference, Vol. 5492, Society of Photo-Optical Instrumentation Engineers (SPIE) Conference Series, ed. A. F. M. Moorwood & M. Iye, 331–340  
 Cooray, A. R. 1999, *A&A*, 341, 653  
 Crain, J. A., Clemens, J. C., & Bayliss, M. 2004, in Presented at the Society of Photo-Optical Instrumentation Engineers (SPIE) Conference, Vol. 5496, Society of Photo-Optical Instrumentation Engineers (SPIE) Conference Series, ed. H. Lewis & G. Raffi, 455–462  
 Dalal, N., Holder, G., & Hennawi, J. F. 2004, *ApJ*, 609, 50  
 D’Aloisio, A., & Natarajan, P. 2011, *MNRAS*, 726  
 Diehl, H. T., et al. 2009, *ApJ*, 707, 686  
 Fassnacht, C. D., Koopmans, L. V. E., & Wong, K. C. 2011, *MNRAS*, 410, 2167  
 Faure, C., et al. 2009, *ApJ*, 695, 1233  
 Fedeli, C., Bartelmann, M., Meneghetti, M., & Moscardini, L. 2008, *A&A*, 486, 35  
 Fedeli, C., Meneghetti, M., Bartelmann, M., Dolag, K., & Moscardini, L. 2006, *A&A*, 447, 419  
 Fedeli, C., Meneghetti, M., Gottlöber, S., & Yepes, G. 2010, *A&A*, 519, A91+  
 Finkelstein, S. L., Papovich, C., Rudnick, G., Egami, E., Le Floch, E., Rieke, M. J., Rigby, J. R., & Willmer, C. N. A. 2009, *ApJ*, 700, 376  
 Flores, R. A., Maller, A. H., & Primack, J. R. 2000, *ApJ*, 535, 555  
 Gilbank, D. G., Gladders, M. D., Yee, H. K. C., & Hsieh, B. C. 2011, *AJ*, 94  
 Gilmore, J., & Natarajan, P. 2009, *MNRAS*, 396, 354  
 Gladders, M. D., Hoekstra, H., Yee, H. K. C., Hall, P. B., & Barrientos, L. F. 2003, *ApJ*, 593, 48  
 Gladders, M. D., & Yee, H. K. C. 2000, *AJ*, 120, 2148  
 —. 2005, *ApJS*, 157, 1  
 Grossman, S. A., & Narayan, R. 1988, *ApJ*, 324, L37  
 Hamana, T., & Futamase, T. 1997, *MNRAS*, 286, L7  
 Hennawi, J. F., Dalal, N., Bode, P., & Ostriker, J. P. 2007, *ApJ*, 654, 714  
 Hennawi, J. F., et al. 2008, *AJ*, 135, 664  
 Hilbert, S., Metcalf, R. B., & White, S. D. M. 2007, *MNRAS*, 382, 1494  
 Hilbert, S., White, S. D. M., Hartlap, J., & Schneider, P. 2008, *MNRAS*, 386, 1845  
 Horesh, A., Maoz, D., Hilbert, S., & Bartelmann, M. 2011, *ArXiv e-prints*  
 Horesh, A., Ofek, E. O., Maoz, D., Bartelmann, M., Meneghetti, M., & Rix, H.-W. 2005, *ApJ*, 633, 768  
 Ilbert, O., et al. 2009, *ApJ*, 690, 1236  
 Kasun, S. F., & Evrard, A. E. 2005, *ApJ*, 629, 781  
 Kazantzidis, S., Kravtsov, A. V., Zentner, A. R., Allgood, B., Nagai, D., & Moore, B. 2004, *ApJ*, 611, L73  
 Koester, B. P., Gladders, M. D., Hennawi, J. F., Sharon, K., Wuyts, E., Rigby, J. R., Bayliss, M. B., & Dahle, H. 2010, *ApJ*, 723, L73  
 Komatsu, E., et al. 2011, *ApJS*, 192, 18  
 Larson, D., et al. 2011, *ApJS*, 192, 16  
 Li, G.-L., Mao, S., Jing, Y. P., Bartelmann, M., Kang, X., & Meneghetti, M. 2005, *ApJ*, 635, 795  
 Li, G. L., Mao, S., Jing, Y. P., Mo, H. J., Gao, L., & Lin, W. P. 2006, *MNRAS*, 372, L73  
 Lowenthal, J. D., et al. 1997, *ApJ*, 481, 673  
 Luppino, G. A., Gioia, I. M., Hammer, F., Le Fèvre, O., & Annis, J. A. 1999, *A&AS*, 136, 117  
 Mead, J. M. G., King, L. J., Sijacki, D., Leonard, A., Puchwein, E., & McCarthy, I. G. 2010, *MNRAS*, 406, 434  
 Meneghetti, M., Bartelmann, M., & Moscardini, L. 2003, *MNRAS*, 346, 67  
 Meneghetti, M., Bolzonella, M., Bartelmann, M., Moscardini, L., & Tormen, G. 2000, *MNRAS*, 314, 338  
 Meneghetti, M., Fedeli, C., Pace, F., Gottlöber, S., & Yepes, G. 2010, *A&A*, 519, A90+  
 Narayan, R., & Bartelmann, M. 1996, *ArXiv Astrophysics e-prints*  
 Oguri, M., Bayliss, M. B., Dahle, H., Sharon, K., Gladders, M. D., Natarajan, P., Hennawi, J. F., & Koester, B. P. 2011, *ArXiv e-prints*  
 Oguri, M., Lee, J., & Suto, Y. 2003, *ApJ*, 599, 7  
 Oguri, M., et al. 2009, *ApJ*, 699, 1038  
 Peng, C. Y., Ho, L. C., Impey, C. D., & Rix, H.-W. 2010, *AJ*, 139, 2097  
 Puchwein, E., Bartelmann, M., Dolag, K., & Meneghetti, M. 2005, *A&A*, 442, 405  
 Puchwein, E., & Hilbert, S. 2009, *MNRAS*, 398, 1298  
 Quider, A. M., Shapley, A. E., Pettini, M., Steidel, C. C., & Stark, D. P. 2010, *MNRAS*, 402, 1467  
 Rauch, M. 1998, *ARA&A*, 36, 267  
 Rigby, J. R., Wuyts, E., Gladders, M. D., Sharon, K., & Becker, G. D. 2011, *ApJ*, 732, 59

- Rozo, E., Nagai, D., Keeton, C., & Kravtsov, A. 2008, *ApJ*, 687, 22
- Schlegel, D. J., Finkbeiner, D. P., & Davis, M. 1998, *ApJ*, 500, 525
- Siana, B., et al. 2009, *ApJ*, 698, 1273
- Smail, I., et al. 2007, *ApJ*, 654, L33
- Springel, V., et al. 2005, *Nature*, 435, 629
- Steidel, C. C., Adelberger, K. L., Shapley, A. E., Pettini, M., Dickinson, M., & Giavalisco, M. 2003, *ApJ*, 592, 728
- Steidel, C. C., Giavalisco, M., Dickinson, M., & Adelberger, K. L. 1996a, *AJ*, 112, 352
- Steidel, C. C., Giavalisco, M., Pettini, M., Dickinson, M., & Adelberger, K. L. 1996b, *ApJ*, 462, L17+
- Steidel, C. C., & Sargent, W. L. W. 1987, *ApJ*, 313, 171
- Steidel, C. C., Shapley, A. E., Pettini, M., Adelberger, K. L., Erb, D. K., Reddy, N. A., & Hunt, M. P. 2004, *ApJ*, 604, 534
- Suh, H., Jeong, H., Oh, K., Yi, S. K., Ferreras, I., & Schawinski, K. 2010, *ApJS*, 187, 374
- Torri, E., Meneghetti, M., Bartelmann, M., Moscardini, L., Rasia, E., & Tormen, G. 2004, *MNRAS*, 349, 476
- Wambsganss, J., Bode, P., & Ostriker, J. P. 2004, *ApJ*, 606, L93
- . 2005, *ApJ*, 635, L1
- Wambsganss, J., Ostriker, J. P., & Bode, P. 2008, *ApJ*, 676, 753
- Wen, Z. L., Han, J. L., & Jiang, Y. Y. 2011, *ArXiv e-prints*
- Williams, L. L. R., & Lewis, G. F. 1996, *MNRAS*, 281, L35
- Wuyts, E., et al. 2010, *ApJ*, 724, 1182
- Yee, H. K. C., Ellingson, E., Bechtold, J., Carlberg, R. G., & Cuillandre, J.-C. 1996, *AJ*, 111, 1783
- York, D. G., et al. 2000, *AJ*, 120, 1579
- Zaritsky, D., & Gonzalez, A. H. 2003, *ApJ*, 584, 691